JOURNAL OF GEOPHYSICAL RESEARCH, VOL. 99, NO. C3, PAGES 5171–5180, MARCH 15, 1994

Microstructure and electrical properties of marine ice and its relationship to meteoric ice and sea ice

John C. Moore

British Antarctic Survey, Natural Environment Research Council, Cambridge, England
Arctic Centre, University of Lapland, Rovaniemi, Finland

Andrew P. Reid

Department of Biology, University of Lancaster, England

Josef Kipfstuhl

Alfred-Wegener Institute for Polar and Marine Research, Bremerhaven, Germany

Abstract. A 215-m ice core has penetrated the central part of the Ronne Ice Shelf (76°59'S, 52°16'W). The core consisted of meteoric ice above 152.8-m depth; below this the ice was bubble free, and of seawater origin. The salinity of the layer below 152.8-m depth is less than 0.05 ppt, very much lower than typical sea ice. The ice represents an unusual source of ice intermediate in salinity and some physical properties between meteoric ice and sea ice. The structure of the ice from four different depths, where salinities vary by a factor of 4, has been investigated using a scanning electron microscope (SEM). The fabric and grain structures are unusual and seem to depend on the impurity concentration in the ice. Chemical impurity localization has also been investigated. The dielectric properties of the ice show that the ice has a transitional behavior from the linear dependence of conductivity on chloride concentration found in meteoric ice, to the less predictable sea ice behavior. The behavior may be interpreted in terms of the structure of the ice. The higher-salinity samples show convoluted grain boundaries, small grain size, and brine inclusions. There are indications that the brine inclusions were liquid at temperatures between -10°C and -30°C. By contrast, the lower-salinity samples possess larger grain sizes and show no evidence of brine inclusions. All samples show brine concentrated at triple grain junctions and also along two-grain boundaries in higher-salinity samples. The dielectric properties of the lower-salinity samples are well described by a Jaccard mechanism with L defects created in proportion to salinity, that also describes the behavior of meteoric ice. Higher-salinity samples exhibit lower conductivity than would be seen if L defects continued to be created in proportion to salinity. The dielectric and structural data are consistent with a solubility limit of about 300 μM for Cl in the ice lattice.

Introduction

In this paper we describe the first electron microscopy analyses on a recently discovered type of ice. The ice, though being formed from frozen seawater, contains very little salt, and is in fact closer to normal meteoric ice in its impurity concentrations. We first describe the general characteristics of the ice and its bulk chemical composition, then the results of structural analysis based on scanning electron microscopy (SEM) and finally, the electrical properties of the ice. We will show that the ice contains unusual structural features that are probably determined by its impurity concentration, which in turn, also determine its electrical properties. The impurity loading of the ice is determined by the ice formation mechanism, and while we do not present a model of the formation process, we do present observations that must be explained in such a complete model.

Paper number 93JC02832.
0148-0227/94/93JC-02832$05.00

Marine Ice

A 215-m-long ice core has been recovered from the central part of the Ronne Ice Shelf (site B13; 76°59'S, 52°16'W, total ice thickness is 239 m [*Oerter et al.*, 1992]) (Figure 1). The top 152.8 m of the core consisted of bubbly ice of meteoric origin. Below this depth the ice changed abruptly to clear bubble-free ice containing layers of entrained particles [*Oerter et al.*, 1992]. The transition corresponded to a radio echo (RES) horizon, taken to be the base of the ice shelf in some earlier surveys [*Robin et al.*, 1983], but later found to be an internal reflector [*Engelhardt and Determann*, 1987; *Thyssen*, 1988]. Measurements of meltwater electrolytic conductivity on drill chips from the core show that the ice below the transition has a much higher conductivity than the ice in the upper part of the core. The higher-conductivity ice corresponds to salinities around 0.05 ppt, higher than meteoric ice (typically up to about 0.01 ppt or 150 μM of Cl), but very much less than typical sea ice salinities (3-20 ppt) [*Weeks and Ackley*, 1982]. Stable isotope, textural, and chemical measurements imply that the ice originated from seawater, *Oerter et al.* [1992], and we call ice from this part of the core "marine ice". Marine ice formation is attributed to the ice pump mechanism [*Robin*, 1979; *Lewis and*

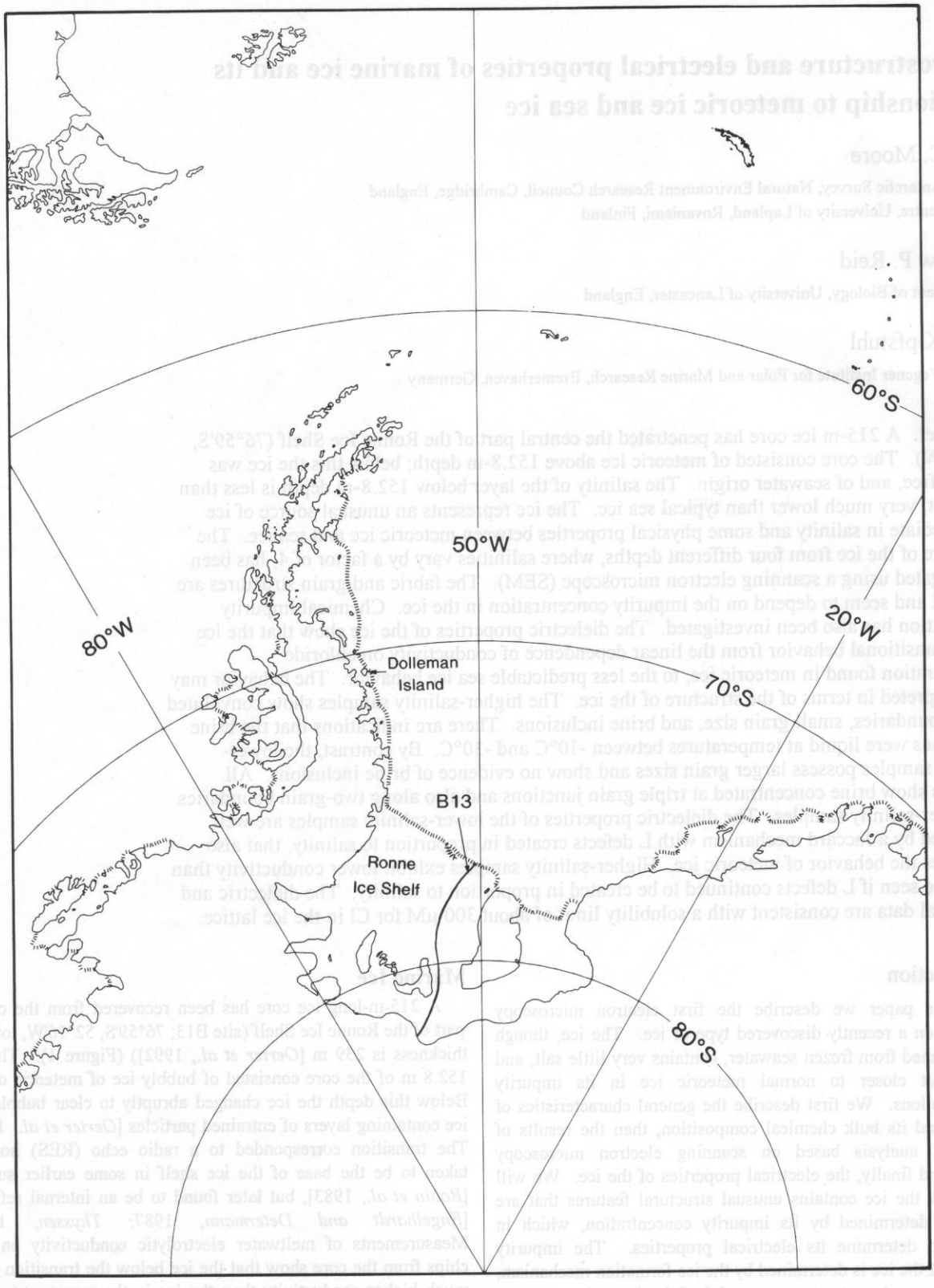

Figure 1. Location map showing Dolleman Island and B13 drilling sites, together with the flowline intersecting the B13 site.

Perkin, 1986]. Melting of ice at depth near the grounding line initiates thermohaline circulation beneath the ice shelf. Frazil ice crystals form in the ascending water mass as it becomes supercooled. The crystals rise and accumulate under the ice shelf, forming a slush layer up to several tens of meters thick [*Engelhardt and Determann*, 1987; *Nicholls et al.*, 1991]. The slush becomes more compact and less saline with time as more ice is aggregated and the brine is squeezed out of the slush. At a critical compaction the slush will become impermeable and the remaining brine will be trapped in the ice. Calculations of brine removal using the mechanisms suggested for sea ice [*Weeks and Ackley*, 1982] cannot remove salt to the degree observed in marine ice [*Eicken et al.*, In Press]. Instead a new hypothesis of brine removal is required, and is under active consideration, but is beyond the scope of this paper. *Oerter et al.* [1992] report that marine ice does not exhibit specific sea-ice characteristics such as brine drainage channels, bubbles, pronounced *c* axis alignments or an evenly spaced substructure. Based on ice velocities on the Ronne ice shelf upstream of the B13 drilling site, the oldest marine ice at the RES horizon is probably between 500 years old [*Oerter et al.*, 1992] and 800 years old (based on flowline modeling by A. Jenkins, personal communication, 1993). The marine ice is up to 300 m thick in some places on the ice shelf [*Engelhardt and Determann*, 1987; *Thyssen*, 1988]. Mass-balance studies and flowline modeling [*Determann et al.*, [1991]; (A. Jenkins, personal communication, 1993) indicate a basal melt rate of 1.5 m yr^{-1} and a thickness of about 100 m for the marine ice layer at the B13 site.

Samples

Ice samples were taken from four depths in the marine ice part of the core (Table 1). The samples represent a 400-year time span [*Oerter et al.*, 1992] and display a range of chemical properties from the oldest, most saline ice near the meteoric/marine ice transition, to less saline ice near the bottom of the core. Crystal size increased with depth down the core (Figure 2), while entrained particle number decreased with depth. At each depth sampled, cross sections of the core were taken for crystal size analysis, dielectric measurements, bulk chemistry and SEM analysis. The dielectric measurements were performed on 1-cm-thick microtomed samples. The samples were measured in a parallel plate electrode apparatus, at -22°C. Chemical samples were taken from immediately above and below the dielectric samples.

Oerter et al. [1992] report that chemical analysis of the B13 core shows that there are significant departures in the relative concentrations of chemical impurities from those present in standard mean ocean water (SMOW). We report chemical analyses of our samples in Table 1. Anions were measured using a Dionex 2010i ion chromatography instrument with an accuracy of 5% and detection limit of about 0.05 μM. Cations were analyzed by flame atomic absorption spectrometry using a Pye Unicam SP9 with 3% precision and 0.1-μM detection limit for Na and 0.05 μM for Mg. The samples were diluted by a factors of 40 for B13 252 and B13 262 and by 10 for the others prior to analysis. Oerter et al. [1992] reported that Na^+ was enriched relative to Cl^-, while SO_4^{2-} and Mg^{2+} were depleted; however, Table 1 shows that Na^+, SO_4^{2-} and Mg^{2+} are depleted in all the four samples that we analyzed. The ratios of $Ca^{2+}$and K^+ to Cl^- show no consistent departures from SMOW ratios, though most data suggest relative depletions. Depletion of SO_4^{2-} has been observed in some percolation areas of the McMurdo Ice Shelf brine zone [*Cragin et al.*, 1986]. As brine percolates through the cold ice of the ice shelf, and is cooled below -8°C, frozen $Na_2SO_4.10H_2O$ crystals remain in situ while the remaining liquid brine percolates further before freezing, leaving parts of the ice shelf enriched and other parts depleted in $SO4^{2-}$. However, Mg^{2+} salts are not thought to freeze in significant quantities above -30°C [*Richardson*, 1976], much colder than the ice in the B13 core has experienced. Thus it seems that precipitation of cryohydrates of any kind cannot account for the observed fractionation.

The mechanism responsible for the fractionation must explain why the degree of chemical fractionation generally increases with depth. Since the production process of frazil ice platelets in the water beneath the ice shelf is probably similar for all the marine ice body, the consolidation process of the slush under the ice shelf is the most likely cause of the fractionation. The consolidation process involves mechanical compaction and also freezing and recrystallization at temperatures close to the melting point. The large anion SO_4^{2-}

Table 1. Physical and Chemical properties of the B13 Ice Core Samples

Sample	B13 252	B13 262	B13 294	B13 322
Depth, m	154.3	159.9	178.95	196.88
Borehole temp. °C	-14.4	-13.9	-12.2	-10.6
Grain vol./area, mm	1.07	1.16	2.06	2.36
Salinity, ppt	0.076	0.055	0.027	0.024
ECM current, μA	0.6	0.1	0.05	0.05
Measured σ_∞, μS m^{-1}	211	192	167	156
Predicted σ_∞*, μS m^{-1}	470-530	340-380	175-200	155-175
Cl^-, μM	1135	811	405	355
SO_4^{2-}, μM	44	26	8.5	9
Na^+, μM	970	602	312	285
Mg^{2+}, μM	90	41	16	14
K^+, μM	37.8	10.9	5.9	-
Ca^{2+}, μM	24	7.3	5.4	4.8
Na^+/Cl^-, (SMOW=0.857)	0.855	0.742	0.770	0.803
Mg^{2+}/Cl^-, (SMOW=0.097)	0.079	0.051	0.040	0.039
SO_4^{2-}/Cl^-, (SMOW=0.052)	0.039	0.032	0.021	0.025

* The 95% confidence interval predicted from (2), the regression analysis of the Dolleman Island data set.

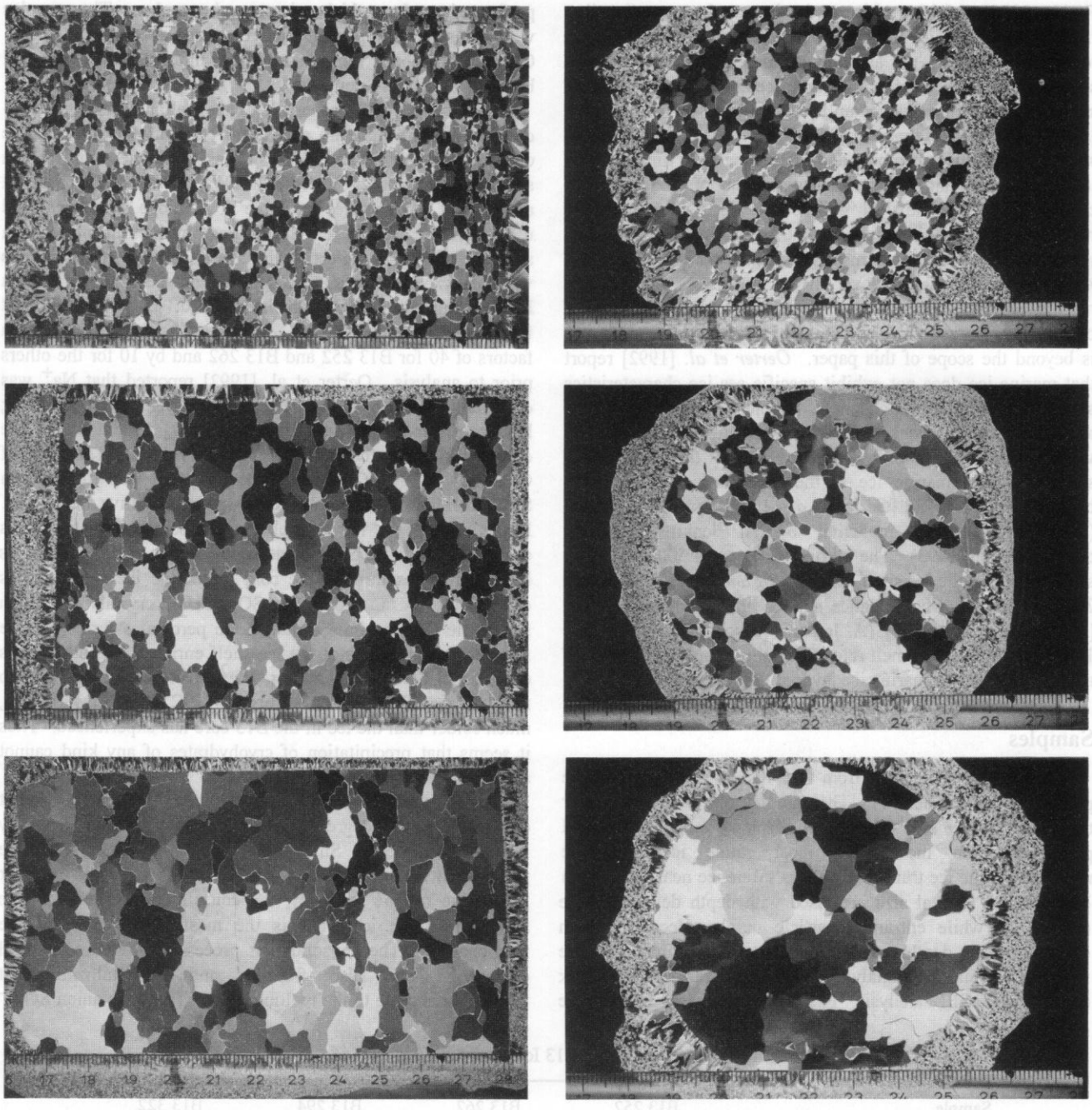

Figure 2. Horizontal (left) and vertical (right) thin sections of the marine ice in the B13 core from (top) 153.5-m (just below the meteoric/marine ice transition), (middle) 173.5-m, and (bottom) 190-m depths, showing the increase in crystal size with depth. The scale is marked in centimeters.

and positively charged cations such as Mg^{2+} with ionic radii much greater than the oxygen center separation in the ice lattice are excluded from the ice crystals more effectively than the much smaller Cl^- ion. The apparent lower depletion of Ca^{2+} and K^+ is difficult to explain by simple ionic size and charge considerations, but other factors such as adsorption onto the surfaces of entrained particles may be important. At slow consolidation rates, Mg^{2+}, Na^+ and SO_4^{2-} excluded from the ice crystals are drained away with the brine, leaving behind Cl^- in the crystals. At faster consolidation rates more brine is trapped within the ice slush zone, and the impurity present in the crystal is a smaller fraction of the impurity trapped in brine pockets, which masks the fractionation effect. These considerations imply that the higher-salinity marine ice samples formed when slush consolidation was quicker than for the lower-salinity samples. This is reasonable, as the temperature gradient in the slush layer at the start of marine ice formation must have been greater than after freezing had progressed longer because of the cold meteoric ice in the ice shelf.

SEM Results

The samples for SEM analysis were from parts of the core a few centimeters above the dielectric samples. Because of their small size (100 mm^3), several samples were prepared from each

depth. The SEM technique used is described in [*Mulvaney et al.*, 1988]. Briefly, the samples were mounted on SEM stubs and microtomed at temperatures around -15°C in Cambridge, and -30°C in Lancaster, then plunged into liquid nitrogen. The sample was coated with about 40 nm of aluminium in a cryochamber under high vacuum ($\approx 5 \times 10^{-6}$ torr), then placed on the cold stage of the electron microscope. Elemental analysis was done using an X ray microprobe at about -160°C. The chemical analysis of ice adjacent to the SEM samples (Table 1) showed impurity levels in all samples were much less than the SEM detection limit of ≈5 mM Cl. Therefore, if the Cl were distributed evenly throughout the samples, no Cl would be detectable. The SEM can only detect Cl in localized areas where concentrations exceed the detection limit. Concentrations can be estimated from the SEM signal count with reasonable accuracy (perhaps ±20%) when the features analyzed are larger than 1 μm [*Reid et al.*, 1992].

The least saline samples (294 and 322) showed grain boundaries very similar in character to those observed in meteoric ice (Figure 3). Two-grain boundaries appeared as sharp lines less than 1 μm wide, triple junctions were also less than 1 μm across. 294 showed Cl at triple junctions, while 322 showed Cl at triple junctions and along many two-grain boundaries. The most saline samples (252 and 262) with the smallest grain size (Table 1) showed evidence of lenslike inclusions and very thick two-grain boundaries (>5 μm) (Figure 4). Elemental analyses (Figure 5) show that the inclusions, triple junctions, circular blobs, and wide two-grain boundaries contain the components of brine.

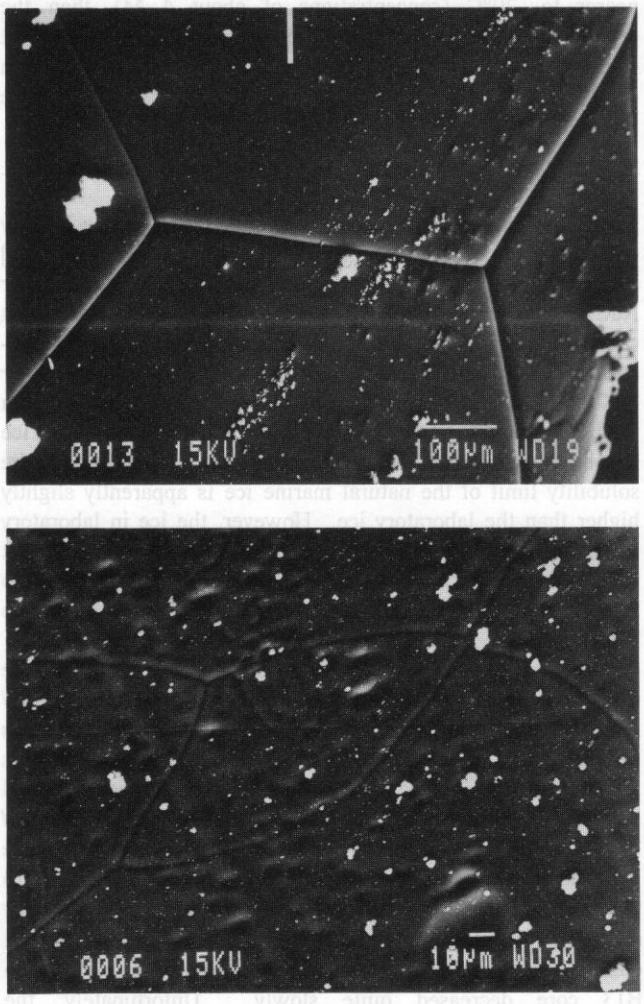

Figure 3. SEM micrograph of normal grain boundaries, seen as dark troughs. The upper micrograph is meteoric ice from Dolleman Island, the lower shows a sample of marine ice. The bright lumps on the surface of the ice are a result of condensation on the ice which became electrically charged in the electron beam.

Very little S was seen in any of the spectra taken across inclusions or triple junctions. As mentioned earlier, SO_4 is depleted relative to SMOW in the samples; however, we should still have detected S in the concentrated brine inclusions. A possible explanation is that the $Na_2SO_4.10H_2O$ crystals containing most of the S should have precipitated from the brine, initially to the boundary walls, at the in situ ice shelf temperature. It would not therefore appear in analyses of the central parts of wide grain boundaries and inclusions. Analyses centered on boundary walls are much less sensitive because of the large area of essentially pure ice sampled by the microprobe.

The blobs appear mainly around the inclusions and are aligned in the direction of microtoming. We interpret these features as spills of liquid caused by the microtoming of the brine-filled inclusions, evidence that the brine was liquid when the samples were microtomed at between -15°C and -30°C. The larger blobs and inclusions were over 10 μm across. Concentrations of Cl found varied between 1 M and 4.5 M, but were typically around 2 M ±0.5 M.

Localized Brine Features

A liquid inclusion will depress the melting point of the two-phase system through three effects: the depression due to the excess hydrostatic pressure in the liquid phase caused by freezing at depth, depression due to increase in Gibbs free energy due to curved concave solid-liquid interfaces, and depression due to impurities. If the bubbles formed near the base of the ice shelf at around 500-m depth [*Thyssen*, 1988], the excess pressure in the bubbles is about 35 bars and the reduction in the melting point is about 0.3°C. For inclusions or grain boundaries of the dimensions observed here the effect of the curved ice-brine interface is less than 0.1°C. The change in melting point due to impurity concentration in the liquid is much larger than the other two effects. NaCl at 2 M concentrations is in equilibrium with ice at -8°C [*Weeks and Ackley*, 1982]. The in situ temperature of the ice was about -12°C. Considering the scattered concentration data from the X ray analyses (2 M ±0.5 M), it is plausible to assume that the brine was at its equilibrium concentration in the ice at the in situ temperature. The samples were left for several hours to reach equilibrium before microtoming, and we may expect that the brine concentration would be appropriate to the microtoming temperature of -15°C to -30°C; however, the measured concentrations are much lower than are required for equilibrium at these temperatures. Irrespective of whether the brine was in true equilibrium with the ice, the blobs (Figure 4) and inclusions do certainly appear to have been liquid when the samples were microtomed. The liquid would have been solidified as soon as the sample was plunged into liquid nitrogen after microtoming. Since the inclusions are all at grain boundaries, it is likely that the brine in the narrower parts of the boundaries was also liquid and in the same equilibrium concentrations. Only minimum concentration estimates are possible for the lower-salinity samples, since the two-grain boundaries and triple junctions are less than 1 μm wide, but measurements are consistent with the

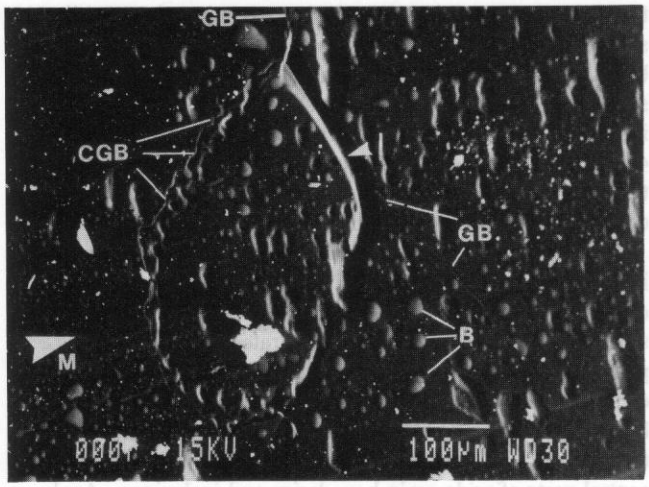

Figure 4. SEM micrograph of brine inclusions and brine blobs on the surface of marine ice. Scratches on the ice surface show the direction of microtoming (M) which is from bottom left to top right. The brine inclusion is located in the curved trough running down the top center of the micrograph (I). A two-grain boundary runs into the inclusion from the top and leaves the inclusion about 3/4 of the way along running towards the bottom right (GB); near the inclusion the boundary is wider than normal. There appears to be a convoluted boundary with several smaller brine inclusions running down the left from the top of the inclusion (CGB). The circular objects (B) with shading on the left half and highlights on the right half are concentrated brine which appear to have been frozen on the ice surface; the blobs are aligned along the direction of microtoming. The shading is consistent with the inclusion being a depression, while the blobs are elevated parts of the surface, interpreted as caused by liquid brine from the inclusions being splashed on the surface during microtoming of the sample, then solidified when the sample was plunged into liquid nitrogen.

assumption that the brine was liquid before it was plunged into liquid nitrogen immediately prior to transfer to the SEM.

We can thus estimate the total Cl localized at grain boundaries and inclusions by calculating the volume of the grain boundary and inclusions, and multiplying by the concentration of Cl. The surface areas of the grains were calculated from the thin sections, and volume to area ratios derived assuming spherical grains. The grain boundary contribution, C_{gb} to the bulk ice concentration is given by

$$C_{gb} = C\, w/r \qquad (1)$$

where C is the *in situ* impurity concentration in the grain boundary, w is the grain boundary width, and r is the grain volume to surface area ratio.

Using the micrographs of the different samples from the four depths, the widths w of the grain boundaries were found. Ice from the most saline two depths was very inhomogeneous, with irregular distributions of inclusions and wide grain boundaries, making accurate estimates of liquid volume at grain boundaries difficult. For samples 294 and 322 and other parts where the grain boundary was less than 1 µm across, the width can be estimated from the Cl signal across the boundary, assuming that the concentration of Cl is the same as in the larger area inclusions. The counts are scaled in proportion to the electron beam area containing the grain boundary; this gave grain boundary widths around 0.3 µm.

This procedure leads to bulk Cl concentrations localized at grain boundaries of 320 µM for sample 252, 290 µM for sample 262, 160 µM for sample 294, and 145 µM for sample 322.

The volume of brine inside inclusions and wide two-grain boundaries that are found in samples 252 and 262 is hard to estimate from the few samples studied. An estimate for 252 yields a volume fraction of 1.5×10^{-4}, which would, if filled with 2 M NaCl account for about 300 µM of Cl. We estimate a similar amount for 262. Therefore the total localized brine in samples 252 and 262 is about 600 µM (300 µM in grain boundaries and 300 µM in inclusions), while for 294 and 322, about 150 µM is localized simply at grain boundaries. Comparing these concentrations to the bulk concentration values in Table 2 leaves about 300 ± 100 µM for all the samples, and we assume this to be the amount dispersed in the grain. Perhaps a larger source of error is the uncertainty of the concentration of the brine in the inclusions. We have assumed a 2 M concentration on the basis of calibration experiments [*Reid et al.*, 1992]. If the concentration was much greater, as might be expected if the brine was in equilibrium with ice at temperatures nearer to -20°C (concentrations of about 4 M), then the calculation of amount dispersed in the grain will be in great error. Fortunately, there are some laboratory experiments on crystal growth and electrical data on the samples discussed here that provide extra support for our calculations.

Dispersed NaCl

We can interpret the above discussion in terms of a solubility limit of Cl in ice of around 300 µM. *Gross et al.* [1977] suggested from laboratory work that a solubility limit existed for NaCl that represented the maximum concentration of salt that could be incorporated in the lattice. The limit found was 100-200 µM, which agreed with earlier work by *Seidensticker* [1972]. The ice grown in the laboratory was grown in a relatively short period compared with the time the marine ice has been *in situ*. It is therefore perhaps surprising that the solubility limit of the natural marine ice is apparently slightly higher than the laboratory ice. However, the ice in laboratory experiments does not undergo the recrystallization process that occurs in natural marine ice and polar ice sheets, and so impurities have only one lattice-building opportunity in which to be incorporated.

The basal ice formation rates beneath the Filchner-Ronne Ice Shelf have been modeled by *Determann* [1991] and *Jenkins and Doake* [1991]. *Determann* [1991] showed that formation rates of more than 2 m yr^{-1} could occur, but that the freezing is restricted to a relatively small area. A. Jenkins (personal communication, 1993) has used his flowline model [*Jenkins and Doake*, 1991] to model the basal accretion and surface accumulation variation along the flowline that intersects the B13 site. The model suggests that marine ice formation rose rapidly to 2 m yr^{-1} for the oldest parts of the B13 core shortly after the onset of freezing; then formation rates for the deeper parts of the B13 core decreased quite slowly. Unfortunately, the observations used to constrain Jenkins model are rather sparse and it is not possible to determine the accretion rates accurately for each of the samples discussed here. The salinity of the samples decreases with depth (Table 1). We postulate that more brine is trapped at faster slush consolidation rates, which depend on the temperature gradients in the slush, which will be highest

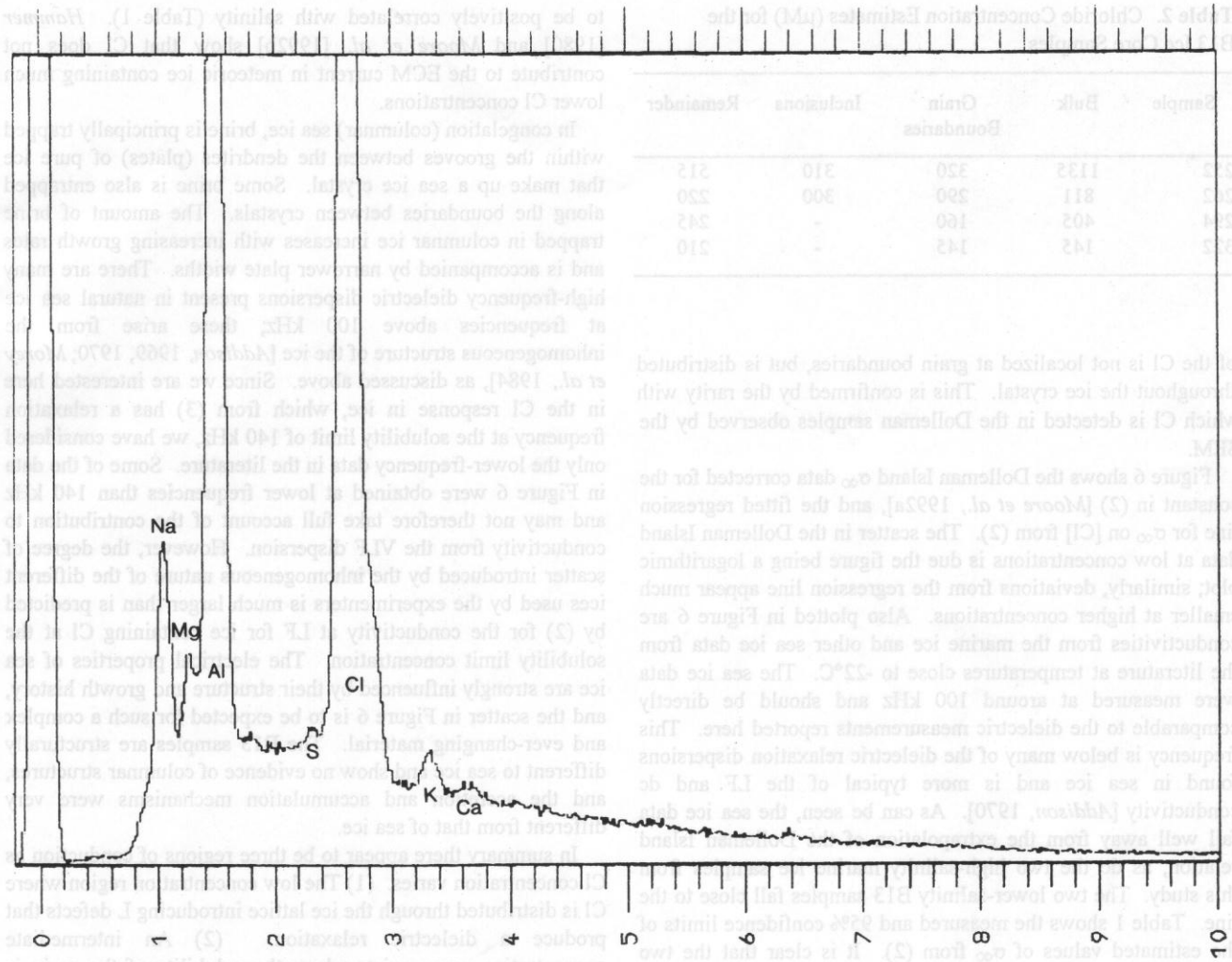

Figure 5. Spectrum taken from the large brine inclusion in Figure 4. The large peak next to Mg is due to Al coating on the sample's surface.

when the slush is thin and close to the cold meteoric ice of the ice shelf. The observed grain size distribution (small grains in old, more saline ice, large grains in younger less saline ice; Figure 2), could be expected to be qualitatively explained by the thermal growth history of the ice. The first ice accreted was rapidly cooled by the cold meteoric ice above and has spent most of its history at cold temperatures. The ice accumulating later spent much longer at temperatures closer to the freezing point, promoting faster grain growth and bigger eventual grain size. However, *Eicken et al.* [In Press] show that thermal history cannot satisfactorily model the crystal size distribution observed. The concentration of impurities, notably Cl^- in meteoric ice, has been postulated as a mechanism for explaining the small grain size of ice from the Wisconsin ice age [*Paterson*, 1991]. It seems likely that impurities, perhaps Cl^- at the grain boundaries, restrict grain growth in marine ice.

Electrical Properties

Moore et al. [1992a] describe conduction mechanisms for ice containing sea-salt impurity based on experimental data from meteoric ice, and also present the temperature dependence of conductivity for the four B13 samples discussed here. In this section we will show how the B13 samples relate to both the well-defined behavior observed for meteoric ice and the much more variable results found for sea ice. *Moore et al.* [1992a] found that the high-frequency limiting value of conductivity σ_∞, and the relaxation frequency f_r of the main VLF Debye dielectric dispersion (see *Moore and Paren*, [1987] for details of experimental procedure) were proportional to Cl concentrations over a range between 1 μM and 100 μM for 806 samples of meteoric ice from Dolleman Island (70°35'S, 60°55'W) (Figure 1), such that at -22°C,

$$\sigma_\infty = (0.43 \pm 0.01)\,[\mathrm{Cl}] + C \quad (2)$$

$$f_r = 8500 + (430 \pm 11)\,[\mathrm{Cl}] \quad (3)$$

where σ_∞ is measured in μS m^{-1}, concentration in μM, f_r in Hz, and C is the contribution to σ_∞ from pure ice. A nonlinear regression analysis on the Dolleman Island data showed that the best fitted power for the dependence of σ_∞ on [Cl] was 0.99, within one standard error of unity, and therefore *Moore et al.* [1992a] took the linear regression model (2).

This behavior has been explained in terms of the Jaccard [e.g., *Hobbs*, 1974] theory of ice conduction. The theory is applicable to processes within the ice lattice, and is consistent with the generation of one Bjerrum L defect for every one to two Cl ions in the ice [*Moore et al.*, 1992a]. This implies that most

Table 2. Chloride Concentration Estimates (μM) for the B13 Ice Core Samples

Sample	Bulk	Grain Boundaries	Inclusions	Remainder
252	1135	320	310	515
262	811	290	300	220
294	405	160	-	245
322	145	145	-	210

of the Cl is not localized at grain boundaries, but is distributed throughout the ice crystal. This is confirmed by the rarity with which Cl is detected in the Dolleman samples observed by the SEM.

Figure 6 shows the Dolleman Island σ_∞ data corrected for the constant in (2) [*Moore et al.*, 1992a], and the fitted regression line for σ_∞ on [Cl] from (2). The scatter in the Dolleman Island data at low concentrations is due the figure being a logarithmic plot; similarly, deviations from the regression line appear much smaller at higher concentrations. Also plotted in Figure 6 are conductivities from the marine ice and other sea ice data from the literature at temperatures close to -22°C. The sea ice data were measured at around 100 kHz and should be directly comparable to the dielectric measurements reported here. This frequency is below many of the dielectric relaxation dispersions found in sea ice and is more typical of the LF and dc conductivity [*Addison*, 1970]. As can be seen, the sea ice data fall well away from the extrapolation of the Dolleman Island relation, as do the two high-salinity marine ice samples from this study. The two lower-salinity B13 samples fall close to the line. Table 1 shows the measured and 95% confidence limits of the estimated values of σ_∞ from (2). It is clear that the two lower-salinity samples are close to the values expected from the Dolleman Island regression analysis, while the two higher-salinity samples are very far away. This is consistent with the presence of most of the Cl in the low-salinity samples in the grain, introducing L defects in the same manner as the Cl in the Dolleman ice. The higher-salinity samples with similar amounts of Cl in the grain (concentrations at the solubility limit) and the remainder at the grain boundaries, conduct less well than predicted from (2).

The Cl at grain boundaries and in inclusions cannot introduce defects in the grain, but contributes to conductivity through disconnected liquid channels and plates. This heterogeneous mixture relaxes due to interfacial polarizations according to the Maxwell-Wagener mechanism [*Addison*, 1970]. The shape and orientation relative to the applied electric field of the brine inclusions and veins are critical in calculating the dielectric relaxation frequency and conductivity of the dispersion. The more spherical the brine inclusion, the higher the relaxation frequency and the smaller its contribution to conductivity.

As the brine concentration is raised, more is forced to the boundaries, until they form continuous linked networks that conduct at dc. The concentration and rate at which the channels become linked are likely to be heavily dependent on ice growth details. More channels will be linked as the salinity increases, giving the positive correlation with the dc conductivity. The ECM [*Hammer*, 1980] (a dc measure of conductivity that depends on acid concentrations in meteoric ice) record of the B13 core (A. Minikin, personal communication, 1993) appears to be positively correlated with salinity (Table 1). *Hammer* [1980] and *Moore et al.* [1992b] show that Cl does not contribute to the ECM current in meteoric ice containing much lower Cl concentrations.

In congelation (columnar) sea ice, brine is principally trapped within the grooves between the dendrites (plates) of pure ice that make up a sea ice crystal. Some brine is also entrapped along the boundaries between crystals. The amount of brine trapped in columnar ice increases with increasing growth rates and is accompanied by narrower plate widths. There are many high-frequency dielectric dispersions present in natural sea ice at frequencies above 100 kHz; these arise from the inhomogeneous structure of the ice [*Addison*, 1969, 1970; *Morey et al.*, 1984], as discussed above. Since we are interested here in the Cl response in ice, which from (3) has a relaxation frequency at the solubility limit of 140 kHz, we have considered only the lower-frequency data in the literature. Some of the data in Figure 6 were obtained at lower frequencies than 140 kHz and may not therefore take full account of the contribution to conductivity from the VLF dispersion. However, the degree of scatter introduced by the inhomogeneous nature of the different ices used by the experimenters is much larger than is predicted by (2) for the conductivity at LF for ice containing Cl at the solubility limit concentration. The electrical properties of sea ice are strongly influenced by their structure and growth history, and the scatter in Figure 6 is to be expected for such a complex and ever-changing material. The B13 samples are structurally different to sea ice and show no evidence of columnar structures, and the accretion and accumulation mechanisms were very different from that of sea ice.

In summary there appear to be three regions of conduction as Cl concentration varies. (1) The low concentration region where Cl is distributed through the ice lattice introducing L defects that produce a dielectric relaxation. (2) An intermediate concentration range exists where the solubility of the grain is reached, no more Cl can be accommodated in the lattice, and excess Cl is forced to grain boundaries. Conduction is through the L defects in the grain and through the dielectric relaxation of the heterogeneous mixture formed by the brine and the ice. (3) The high Cl concentration regime is where the liquid brine channels become linked in a network that starts to conduct at dc. Conductivity depends on the channel geometry and ice history much more strongly than Cl concentration.

Conclusion

We have shown that the marine ice is an interesting and new category of ice with chemical and electrical properties intermediate between meteoric and sea ice. Chemical analysis of the brine shows that Na^+, Mg^{2+}, and SO_4^{2-} are progressively depleted with depth relative to Cl^-, the less saline ice being relatively the most depleted. SEM analyses reveal that the more saline samples contain significant quantities of brine that are localized at inclusions and along grain boundaries. The evidence is consistent with a solubility limit of about 300 μM for Cl in the ice lattice. The more saline samples near to the meteoric ice interface were formed under a higher temperature gradient than the deeper less saline samples, probably leading to faster solidification of the marine ice, causing brine to be trapped in inclusions and at thickened grain boundaries. Exclusion of the ions other than Cl^- from the ice crystal lattice can partly explain the observed chemical fractionation.

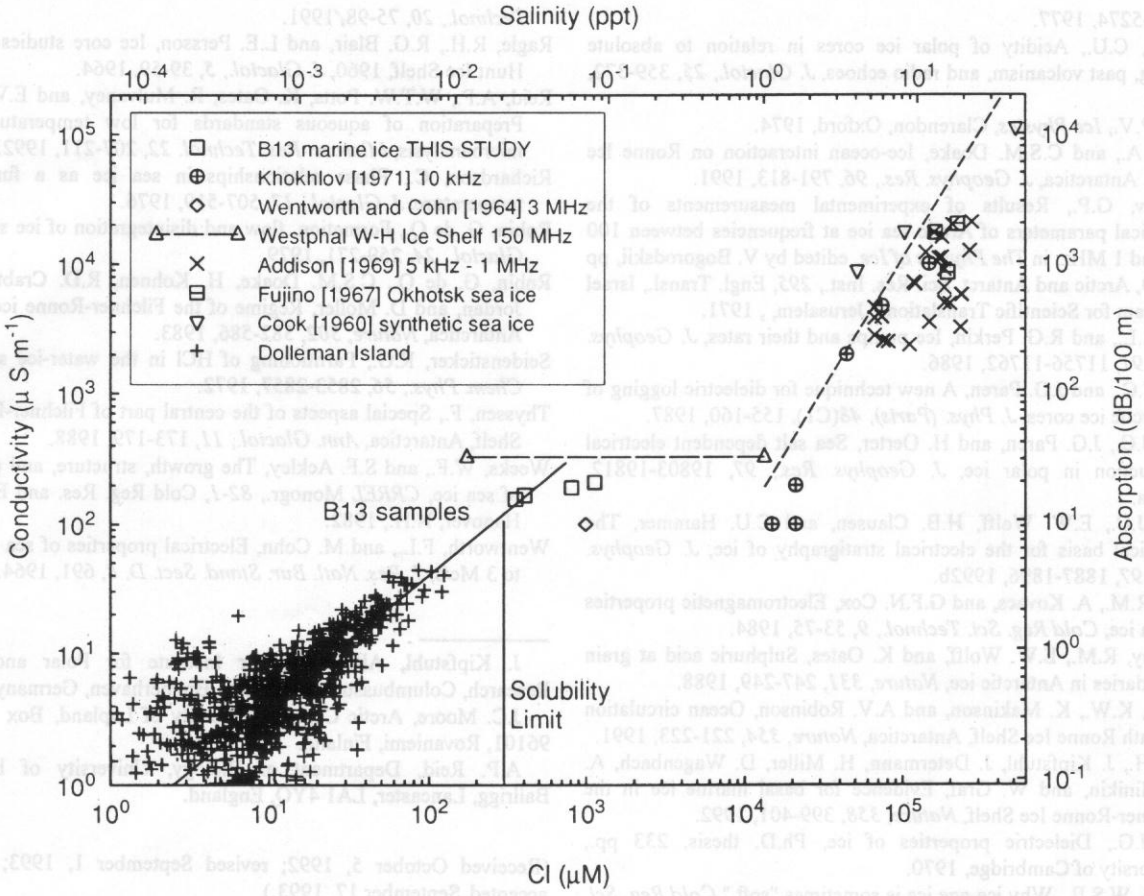

Figure 6. Logarithmic plot of conductivity (absorption) versus Cl concentration (salinity) at -22°C for samples of meteoric ice, marine ice, and sea ice. The solid line is the regression line found for the Dolleman samples (2). The scatter in the Dolleman data at low values appears great due to the logarithmic scales. The two lower-salinity B13 samples lie very close to the regression line, while the two higher-salinity samples are have very significantly lower conductivities than are expected from (2); see Table 1. The short-dashed line is a form line only with conductivity proportional to the square of salinity. Sea ice data were selected at the temperature of measurement closest to 22°C, and at frequencies close to 100 kHz (actual frequencies measured are indicated in the key). The long-dashed line between Westphal's data points represents two Cl concentrations reported for the same sample by different authors [*Ragle et al.*, 1964; *Paren*, 1970].

Dielectrically, the marine ice is also intermediate between meteoric ice and sea ice. Ice with Cl concentrations less than the solubility limit exhibits the same linear dependence of high-frequency conductivity on Cl concentrations as meteoric ice, which can be explained by the generation of point defects in the ice lattice. Higher-salinity ice does not behave in the same way due to the exclusion of brine from the lattice to the grain boundaries, which conducts via Maxwell-Wagener interfacial polarizations.

Acknowledgments. We thank A. Minikin for providing his ECM data on the core. Valuable comments from A. Jenkins and K. Nicholls helped the oceanography aspects of this paper, and two anonymous referees suggested many improvements to the paper. R. Mulvaney kindly contributed sample preparation and SEM expertise; E. Pasteur and G. Coulson performed the chemical analyses.

References

Addison, J.R., Electrical properties of saline ice, *J. Appl. Phys.*, *40*, 3105-3114, 1969.

Addison, J.R., Electrical relaxation in saline ice, *J. Appl. Phys.*, *41*, 55-63, 1970.

Cook, J.C., RF electrical properties of salty ice and frozen earth, *J. Geophys. Res.*, *65*, 1767-1771, 1960.

Cragin, J.H., A.J. Gow, and A. Kovacs, Chemical fractionation of brine in the McMurdo Ice Shelf, Antarctica, *J. Glaciol.*, *32*, 307-313, 1986.

Determann, J., Numerical modelling of ice shelf dynamics, *Antarct. Sci.*, *3*, 187-195, 1991.

Determann, J., K. Grosfeld, and B. Ritter, Melting rates at the bottom of Filchner-Ronne Ice Shelf, Antarctica, from short-term mass-balance studies, *Polarforschung 60*, 25-32, 1991.

Eicken, H., H. Oerter, H. Miller, W. Graff and J. Kipffstuhl, Textural characteristics and impurity content of meteoric and marine ice in the Ronne Ice Shelf, Antarctica, *J. Glaciol.*, In Press.

Engelhardt, H., and J. Determann, Borehole evidence for a thick layer of basal ice in the central Ronne Ice Shelf, Antarctica, *Nature*, *327*, 318-319, 1987.

Fujino, K., Electrical properties of sea ice, in *Physics of Snow and Ice*, edited by H. Oura, pp. 633-648, Institute of Low Temperature Science, Hokkaido University, Japan 1967.

Gross, G.W., P.M. Wong, and K. Humes, Concentration dependent solute redistribution at the ice-water phase boundary, III, Spontaneous convection, Chloride solutions, *J. Chem. Phys.*, *67*,

5264-5274, 1977.

Hammer, C.U., Acidity of polar ice cores in relation to absolute dating, past volcanism, and radio echoes, *J. Glaciol., 25*, 359-372, 1980.

Hobbs, P.V., *Ice Physics*, Clarendon, Oxford, 1974.

Jenkins, A., and C.S.M. Doake, Ice-ocean interaction on Ronne Ice Shelf, Antarctica, *J. Geophys. Res., 96*, 791-813, 1991.

Khokhlov, G.P., Results of experimental measurements of the electrical parameters of Arctic sea ice at frequencies between 100 Hz and 1 MHz, in *The Physics of Ice*, edited by V. Bogorodskii, pp 64-70, Arctic and Antarct. Sci. Res. Inst., *295*, Engl. Transl., Israel Program for Scientific Translations, Jerusalem, , 1971.

Lewis, E.L., and R.G. Perkin, Ice pumps and their rates, *J. Geophys. Res., 91*, 11756-11762, 1986.

Moore, J.C., and J.G. Paren, A new technique for dielectric logging of Antarctic ice cores, *J. Phys. (Paris), 48*(C1), 155-160, 1987.

Moore, J.C., J.G. Paren, and H. Oerter, Sea salt dependent electrical conduction in polar ice, *J. Geophys. Res., 97*, 19803-19812, 1992a.

Moore, J.C., E.W. Wolff, H.B. Clausen, and C.U. Hammer, The chemical basis for the electrical stratigraphy of ice, *J. Geophys. Res., 97*, 1887-1896, 1992b.

Morey, R.M., A. Kovacs, and G.F.N. Cox, Electromagnetic properties of sea ice, *Cold Reg. Sci. Technol., 9*, 53-75, 1984.

Mulvaney, R.M., E.W. Wolff, and K. Oates, Sulphuric acid at grain boundaries in Antarctic ice, *Nature, 331*, 247-249, 1988.

Nicholls, K.W., K. Makinson, and A.V. Robinson, Ocean circulation beneath Ronne Ice Shelf, Antarctica, *Nature, 354*, 221-223, 1991.

Oerter, H., J. Kipfstuhl, J. Determann, H. Miller, D. Wagenbach, A. A. Minikin, and W. Graf, Evidence for basal marine ice in the Filchner-Ronne Ice Shelf, *Nature, 358*, 399-401, 1992.

Paren, J.G., Dielectric properties of ice, Ph.D. thesis, 233 pp., University of Cambridge, 1970.

Paterson, W.S.B., Why ice-age ice is sometimes "soft," *Cold Reg. Sci. Technol., 20*, 75-98, 1991.

Ragle, R.H., R.G. Blair, and L.E. Persson, Ice core studies of Ward Hunt Ice Shelf, 1960, *J. Glaciol., 5*, 39-59, 1964.

Reid, A.P., W.T.W. Potts, K. Oates, R. Mulvaney, and E.W. Wolff, Preparation of aqueous standards for low temperature X-ray microanalysis, *Microsc. Res. Technol. 22*, 207-211, 1992.

Richardson, C., Phase relationships in sea ice as a function of temperature, *J. Glaciol., 17*, 507-519, 1976.

Robin, G. de Q., Formation, flow and disintegration of ice shelves, *J. Glaciol., 24*, 259-271, 1979.

Robin, G. de Q., C.S.M. Doake, H. Kohnen, R.D. Crabtree, S.R. Jordan, and D. Moller, Regime of the Filchner-Ronne ice shelves, Antarctica, *Nature, 302*, 582-586, 1983.

Seidensticker, R.G., Partitioning of HCl in the water-ice system, *J. Chem. Phys., 56*, 2853-2857, 1972.

Thyssen, F., Special aspects of the central part of Filchner-Ronne Ice Shelf, Antarctica, *Ann. Glaciol., 11*, 173-179, 1988.

Weeks, W.F., and S.F. Ackley, The growth, structure, and properties of sea ice, *CRREL* Monogr., *82-1*, Cold Reg. Res. and Eng. Lab., Hanover, N.H., 1982.

Wentworth, F.L., and M. Cohn, Electrical properties of sea ice at 0.1 to 3 Mc/s, *J. Res. Natl. Bur. Stand. Sect. D, 8*, 691, 1964.

J. Kipfstuhl, Alfred-Wegener Institute for Polar and Marine Research, Columbusstrasse, D 2850, Bremerhaven, Germany.

J.C. Moore, Arctic Centre, University of Lapland, Box 122, FIN 96101, Rovaniemi, Finland.

A.P. Reid, Department of Biology, University of Lancaster, Bailrigg, Lancaster, LA1 4YQ, England.

(Received October 5, 1992; revised September 1, 1993; accepted September 17, 1993.)